

## SPECIAL ISSUE PAPER

## Separation and enhancement of gear and bearing signals for the diagnosis of wind turbine transmission systems

Nader Sawalhi<sup>1</sup>, Robert B. Randall<sup>2</sup> and David Forrester<sup>3</sup>

<sup>1</sup> College of Engineering, Prince Mohammad Bin Fahd University, The Kingdom of Saudi Arabia

<sup>2</sup> School of Mechanical and Manufacturing Engineering, The University of New South Wales, Australia

<sup>3</sup> Defence Science and Technology Organisation, Australia

### ABSTRACT

This paper is based on the analysis of a wind turbine vibration data provided by the National Renewable Energy Laboratory under a round robin scheme to diagnose faults in a transmission that had experienced a loss of lubricant for a period. Previously developed techniques were applied, but this is the first time that some were used in combination for a machine covering such a wide speed range and with such a low minimum speed. Another factor was that the gearbox design was far from ‘hunting tooth’, and this gave problems with the diagnosis. The paper describes how the techniques were adapted to solve these problems. The algorithms used for the diagnosis included the extraction of a pseudo-encoder signal from the vibration signals themselves, to allow order tracking and resampling in the rotation angle domain. This permitted successive resampling over several stages to give synchronous averages for each shaft in the planetary gearbox, allowing diagnostics of the gears on that shaft. Subtraction of all synchronously averaged signals leaves a residual signal containing bearing signals and allowing diagnosis of their faults. This is the first reported case of applying that technique over four separate stages. Bearing diagnosis was carried out using a semi-automated algorithm based on whitening the residual signal, filtering it to maximize the kurtosis and finally using the Hilbert transform approach to get the spectrum of the squared envelope. The analysis of the gears included using spectrum and cepstrum comparisons between healthy and faulty data. It is shown for the first time that cepstra from the same signal (from spectra in different frequency ranges) gives information about completely different gears at very different speeds. The analysis also involved obtaining synchronous averages for the individual planetary gears and for the sun gear by using software patented by the Australian Defence Science and Technology Organisation. The signal processing tools used for the analysis were shown to be capable of identifying both gear and bearing faults in the wind turbine gearbox, though one bearing fault was missed. Copyright © 2013 John Wiley & Sons, Ltd.

### KEYWORDS

diagnosis; gears; rolling element bearings; pre-whitening; synchronous average; cepstrum; pseudo-encoder

### Correspondence

Robert B. Randall, School of Mechanical and Manufacturing Engineering, The University of New South Wales, Australia

E-mail: b.randall@unsw.edu.au

Received 17 March 2013; Revised 18 August 2013; Accepted 20 August 2013

### 1. INTRODUCTION

This paper discusses the analysis of wind turbine vibration data provided by the National Renewable Energy Laboratory (NREL) for the condition monitoring round robin study. NREL provided three sets of data (taken from a number of accelerometers on the planetary gearbox shown in Figure 1), which had a number of naturally occurring faults (gears and bearings). The data was provided at two different relatively constant speeds, 20 Hz (six-pole operation) and 30 Hz (four-pole operation), and two different relatively constant loads (25% and 50% of the rated load). The vibration data, initially provided, was for faulty condition only, but later healthy spectrum data at the highest load was made available that greatly helped in gear diagnosis. It is worth mentioning here that bearing signals (in contrast to gear signals) are not so sensitive to load, and there is usually a dramatic difference in the signals in the presence of faults, which often allows them to be diagnosed without necessarily having access to historical data.

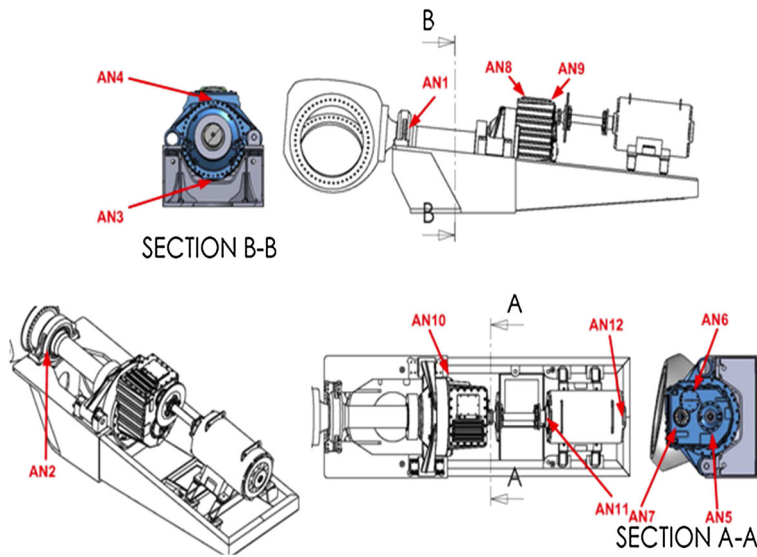


**Figure 1.** Vibration data acquisition system sensor locations.

A number of signal processing algorithms were employed for identifying the faulty components.<sup>1–12</sup> Bearing diagnoses were partially based on a semi-automated procedure, with several different stages to separate and enhance the bearing signals. Then envelope analysis was applied (spectrum analysis of squared envelope signals) to diagnose the fault repetition frequencies and their modulations by lower frequencies.<sup>1</sup> A recently developed pre-whitening technique, which can circumvent some of the stages in the earlier procedure, was also used.<sup>2</sup> Even though the different procedures had been used previously on helicopter gearboxes, this was the first time that the overall combination had been used for a wind turbine gearbox, which differs primarily in that the speed is lower by a factor of more than 10.

For gear diagnosis, spectrum comparisons were performed to detect changes in gear mesh harmonics and modulation sideband patterns. The cepstrum was used as a means to concentrate the information from the sideband patterns and verify the findings. It is shown for the first time that the information in the cepstra is very different when obtained from spectra over different frequency ranges, thus allowing diagnostics of different gears from the same signal. Some classic techniques based on obtaining a synchronously averaged signature for each gear were also applied. The synchronously averaged signatures were scanned for localized impulses, which characterize local faults. This type of processing requires the signals to be ‘order tracked’, or resampled in the angular domain, with equal numbers of samples in each revolution. This normally requires a tachometer or shaft encoder signal for synchronization. The supplied speed signal was not suitable for this so the extraction of a ‘pseudo-encoder’ signal from the vibration signal itself had to be carried out and then used for order tracking. For obtaining signatures of the individual planet gears and sun gear in the planetary part of the gearbox, the premium current method is one patented by Defence Science and Technology (DSTO), of the Australian Defence Department. Dr David Forrester of DSTO, who is the inventor of the technique, obtained these signatures, which are discussed and presented here. It should be mentioned that Dr Forrester expressed his concern at the design of the planetary section of the gearbox, as the choice of tooth numbers was far from a ‘hunting tooth’ design, normally considered good practice, and as a result of this, groups of teeth always mesh in the same way and repeat frequently. It is also somewhat unusual that the ratio of the high-speed (HS) section was exactly 4:1 (88:22) meaning that the 22 teeth on the pinion always mesh in exactly the same way with four groups of 22 teeth on the intermediate shaft wheel. Therefore, a fault on one tooth transfers to individual teeth on the mating gear, and is not smeared out as it is in a hunting tooth design, where the numbers of teeth on meshing gears have no common factors. The effects of this on making the diagnoses more difficult are discussed and illustrated in this paper.

The paper is organized as follows: in Section 2, a summary of the processing algorithms is provided. In Section 3, the results for both the bearing and gear diagnoses are presented and discussed. Finally, Section 4 gives the discussion and conclusions.

## 2. A SUMMARY OF THE PROCESSING ALGORITHMS

The main general approach used in this paper is to separate the vibration signal into the components coming from the gears and bearings and then to analyse and handle them separately.

The separation between the gear and bearing signals is based on the assumption that gear signals are deterministic (with respect to rotation angle) while bearing signals are stochastic because of the minor random slip between the components and the random positioning of the rolling elements in the clearance of the cage.<sup>3</sup> These two effects give an approximately 1–2% deviation of the mean value of the actual bearing fault frequencies, with the same order of random variation around the mean, from those frequencies calculated on the basis of no slip and perfectly uniform spacing. The signals can then be classified as approximately second-order cyclostationary, which allows their separation from the deterministic gear components.<sup>3</sup> There are a number of methods for achieving this separation,<sup>4</sup> but the one initially used in this paper was to first isolate and then remove the deterministic components corresponding to each gear in the system, by synchronous averaging, leaving a residual stochastic signal, which should be dominated by bearing faults in some frequency bands. Although this has been proposed by the authors earlier,<sup>4</sup> this is the first known case where it has been applied over four successive stages to obtain a residual signal. The three basic steps describing the main processing algorithm used in this approach are shown in Figure 2.

The first stage of processing (see Section 2.1) involves extracting a pseudo-tachometer/encoder (tacho) signal (for the resampling process) from the measured vibration signal. This step was necessary as the speed signal provided by NREL was only useful for giving an arithmetic mean estimate of the speed of the HSS (generator rotor) and could not be used for resampling purposes.

The second stage (described in Section 2.2) included the extraction of synchronous averages for each shaft through successive resampling based on the gear ratios. The extracted tacho signal from step one was used to resample the signal of interest and extract the synchronous average for the intermediate shaft. This was successively resampled to obtain a synchronous average for the low speed shaft (sun gear shaft), a composite average for the planet gears and an average over the planet carrier rotation (i.e. input speed), thus corresponding to the ring gear. These synchronously averaged signals were inspected for faults in the gears and then analysed in detail as discussed in Section 3.2.1. For bearing fault detection, the residual signal (raw signal minus all synchronous averages) was pre-whitened as a first step. The squared envelope spectrum was then obtained using the Hilbert transform approach and scanned for bearing defect frequencies (see Section 2.3), which had been calculated for each bearing in the gearbox.

## 2.1. Pseudo-encoder extraction and speed estimation

There are two main methods for performing angular resampling based on a pseudo-encoder signal extracted from the vibration signal, for example, by using a gear mesh signal as a phase-locked shaft harmonic. Method one –which is usually best when there are relatively large speed variations, because it can be repeated iteratively<sup>5</sup>– is based on phase demodulating the component after it is separated by bandpass filtering. This provides a map of phase (shaft rotation angle) versus time, sampled at uniform time intervals. The signals are resampled at uniform phase intervals. With large speed variations, it is often only the low harmonics that are separated, and it is necessary to compensate for the major variations on the basis of these and then iteratively progress to higher harmonics to achieve finer speed correction. In this study, the generator was a squirrel cage induction machine, so speed variations were relatively small, and an alternative method (method 2) proposed by the authors in the following reference<sup>6</sup> could be used. Method 2 is described schematically in Figure 3.

In the first step, Figure 3(a), the spectrum of the signal is visually examined to identify a clear HS shaft (HSS) gear mesh harmonic (and a suitable band around it). Highest separable harmonics are preferable due to the greater effect of smearing,

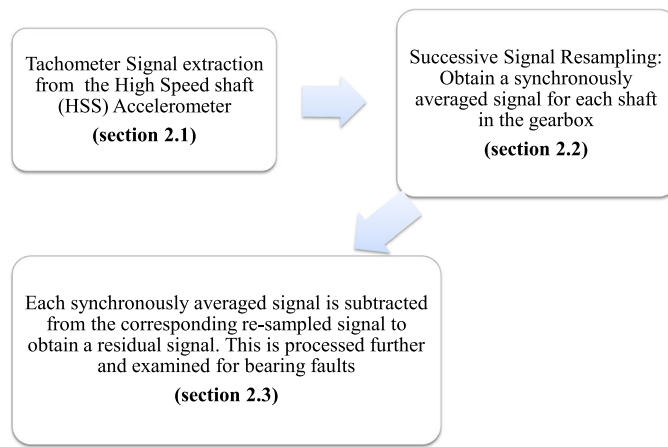
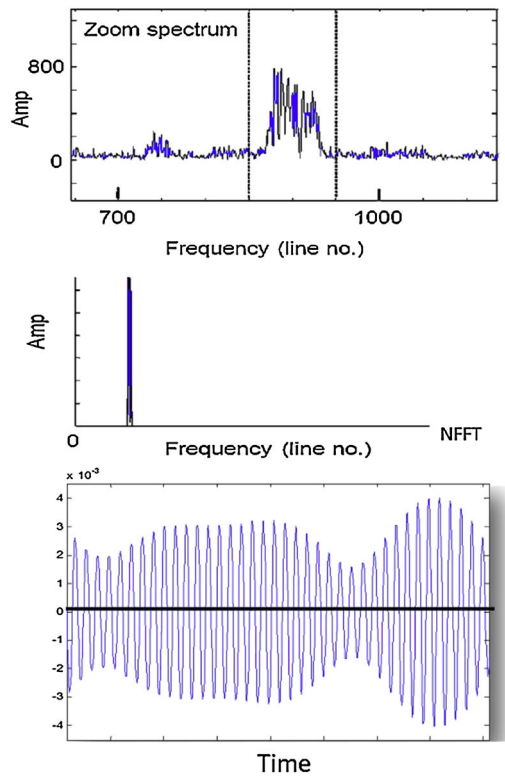


**Figure 2.** Signal processing approach for fault detection in bearings.

**(a) Step 1: Identifying the band of interest. Plot shows the amplitude of the spectrum. Frequency axis scaled in lines rather than Hz**



**(b) Step 2: Band of interest moved into a buffer filled with zeros**

**(c) Step 3: Real part of the IFFT (Inverse Fast Fourier Transform) of the buffer obtained in step 2**

**Figure 3.** Reference (speed) signal extraction stages (a) identifying a separable band, (b) extracting the band into a new buffer and (c) inverting the transform signal b into the time domain (zoomed in).<sup>5</sup>

and the fact that information is only contained about modulation frequencies up to half the frequency used as a reference, and this will give more accurate results, but they should not overlap with other spectral components. In the second step, Figure 3(b), a buffer (filled with zeros) of a size equal to the original fast Fourier transform (FFT) size is created. The complex spectrum of interest (band) is transferred to this buffer (placed in the same lines as in the original spectrum). Note that the presentation in Figure 3(b) only shows the amplitude of the spectrum; however, it is the complex spectrum that is transferred to this buffer, and the phase information is thus preserved. In principle, the amplitude of these frequency components should be multiplied by 2 to maintain the scaling of the resulting time signal, but this is not necessary when only the phase information is required. Finally, the buffer is inverse transformed to the time domain to obtain the reference signal, Figure 3(c). As the buffer is filled with zeros up to the sampling frequency – negative frequencies were set to zero – the inverse transform signal is analytic (complex), and it is the real part that will then represent the reference signal. Note that zero crossings represent 180° increments in the phase of that component, and this is unaffected by amplitude modulation by any positive modulating function.

The signal obtained in Figure 3(c) is a sinusoidal-type signal whose periods represent the reciprocal of the speed for each cycle. The speed variation in this signal (a reflection of the speed variation of the shaft under investigation) can be traced by detecting the zero crossings (an interpolation between the samples on either side). Each zero crossing represents a 180° increment in phase. This phase/time map can then be used to order track the signal.

The approach illustrated in Figure 3 was applied on the data taken from sensor AN7 (placed on the HSS bearing) to extract a tachometer and speed signal for the HSS of the gearbox, although others in close proximity to the HSS could have been used. The speed extraction was based on the gear mesh frequency of the HS stage ( $22 \times$  HSS). Examples of estimates at two speeds (four-pole and six-pole operation) based on this procedure are presented in Figure 4 (scaled in rpm). It is noted that the speed is relatively constant.

## 2.2. Successive resampling and synchronous average extraction

A separation algorithm (gear/bearing signal separation),<sup>7</sup> which is based on successive resampling of the signal under analysis, has been used here to obtain synchronously averaged signals for each shaft and to completely remove the corresponding shaft harmonics with minimum disruption of the residual vibration signal.

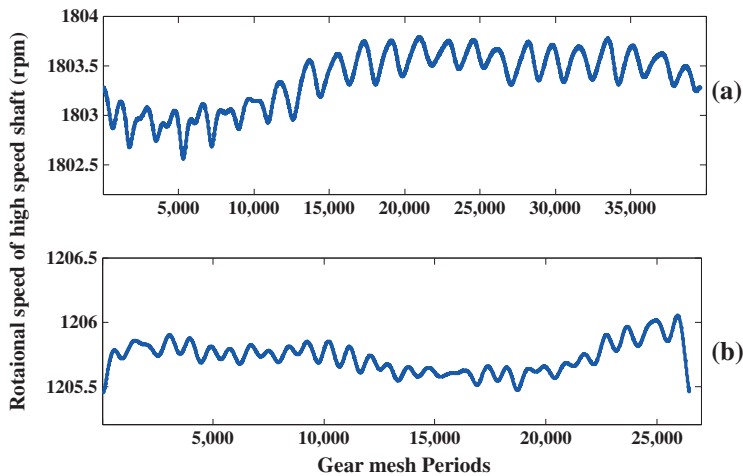


**Figure 4.** High-speed shaft estimates by using sensor AN7. (a): data 2c:5 (set 2c, 5th minute) and (b): data 2a:5 (set 2a, 5th minute).

The algorithm works by resampling the order-tracked signal to obtain an integer number of samples per revolution for a specific shaft. The extracted tacho signal was first used to extract the synchronous average for the intermediate shaft. As the HSS and the intermediate-speed shaft (ISS) have a ratio of four, the removal of the harmonics of HSS was included at this stage. The end result of this stage, after repeating the procedure, was four synchronously averaged signals for the ISS, low-speed shaft, the planet carrier shaft, and the planetary gears (a composite of all the planetary gears; this was later updated to extract an average for each planetary gear). Typical results for the four synchronously averaged signals are presented in Figure 5 for six-pole (1200 rpm) operation.

Initially, no definite conclusions could be reached as to the condition of the gears, in particular because no time signals were available for the gears in good condition, and it is usual to base gear diagnostics on differences from the original condition. Even without comparison, local faults can sometimes be detected by removing the regular gear meshing pattern, which may be masking the local faults,<sup>8</sup> but this simple approach was initially inconclusive. The signals were later subjected to the most powerful analysis technique for planetary gears, based on algorithms patented by DSTO, and this is described in Section 3.2.2.<sup>12</sup>

### 2.3. Residual signal processing for bearing fault detection

After the removal of all the synchronously averaged signals, a residual signal is obtained. This should contain nonstationarities and second-order cyclostationary components. Two main processing steps were carried out on the residual signal, which included pre-whitening this signal and obtaining the squared enveloped spectrum of the pre-whitened signal.

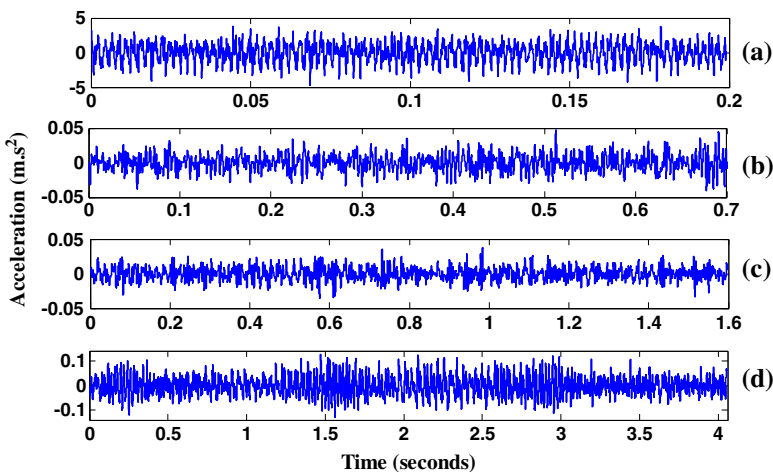


**Figure 5.** Synchronously averaged signals (one complete revolution of each shaft/gear) from for the 5th minute from sensor AN3, data 2a. (a) Intermediate shaft, (b) low-speed shaft, (c) planet gear and (d) planet carrier.

In order to enhance the residual signal and maximize its impulsiveness, a newly proposed pre-whitening approach was used.<sup>2</sup> In this approach, the real cepstrum is set to zero (spectrum amplitude set to one, i.e. whitened). This simultaneously nullifies the effect of both discrete frequencies (although here, the discrete frequency components were already removed) and resonances, so that a frequency band containing an impulsive signal will tend to dominate the time signal. This procedure can alternatively be implemented by simply dividing the Fourier transformed spectrum by its absolute value and transforming back to the time domain; thus giving a uniform spectrum weighting. This uniform weighting means that impulsive frequency bands dominate the time signals and an envelope analysis can be carried out on the full frequency bandwidth. This in turn minimizes the need to search for an optimum frequency band for the envelope analysis, although applying a kurtogram<sup>9</sup> for this purpose can be used as an extra step to enhance impulsiveness even more and was carried out here.

In the second step, the squared envelope spectrum for the pre-whitened residual signal was obtained using Hilbert Transform techniques (simply by inverse transforming one-sided spectra, shifted to zero frequency, and taking the squared modulus of the resulting complex numbers).<sup>10</sup> The spectrum of the squared envelope was inspected for bearing faults.

## 3. RESULTS

### 3.1. Bearings

#### 3.1.1. Bearing diagnosis result

Only one of two possible bearing faults was identified, this being on the downwind bearing of the HSS of the gearbox. It was found on inspection to be discolored by overheating to about 400°F. The photograph in Figure 6<sup>13</sup> shows very minor marks and pits on the inner race as well as the rollers.

The envelope analysis carried out did show components at ballpass frequency, inner race (BPFI) and fundamental train frequency (FTF or cage frequency), which could be partly because of geometric distortion as a result of the overheating. Figure 7 shows a typical result for six-pole operation (20.1 Hz shaft speed), but a very similar result was found for signals from different sensors and also for four-pole operation (30 Hz shaft speed). The harmonics of BPFI in Figure 7 were clearly modulated by the HSS speed, as is typical of inner race faults because it is the rate at which the fault passes through the load zone. The calculated BPFI for the thrust bearing at a shaft speed of 20.06 Hz is around 231 Hz, and this is found in Figure 7.

The FTF (or cage speed) of this bearing for 30 Hz shaft speed was also identified, though weakly, at 12.81 Hz (Figure 8). This represents variations for every rotation of the cage, and could also be explained by the thermal distortion.

#### 3.1.2. Missed detection

The inner race of the upwind bearing on the intermediate shaft had assembly damage at the roller spacing caused by cocking of the rollers during blind assembly. Debris dents and lines of false brinelling were also observed as well as corrosion at roller spacing. No evidence was found of the damage in this bearing. It is possible that there was not a good transmission path from this bearing to the measurement points.

### 3.2. Gears

The diagnostic approaches included comparing the signals with faults present to those in healthy condition in both the frequency domain and in the cepstrum domain. Additionally, synchronous averages were extracted for the sun gear, the ring gear, and each planet gear, from the data with faults, by using an algorithm developed earlier by DSTO.



**Figure 6.** Photos of the inner race and rollers of the high-speed shaft downwind bearing.<sup>13</sup>

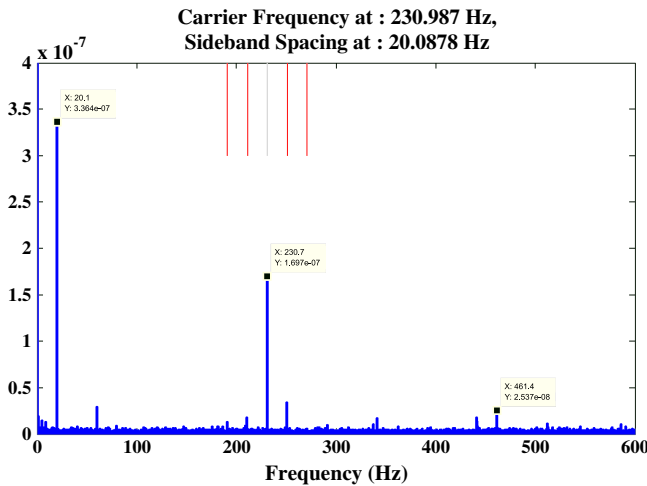


**Figure 7.** Squared envelope spectrum for high-speed shaft thrust bearing at 20.1 Hz shaft speed.

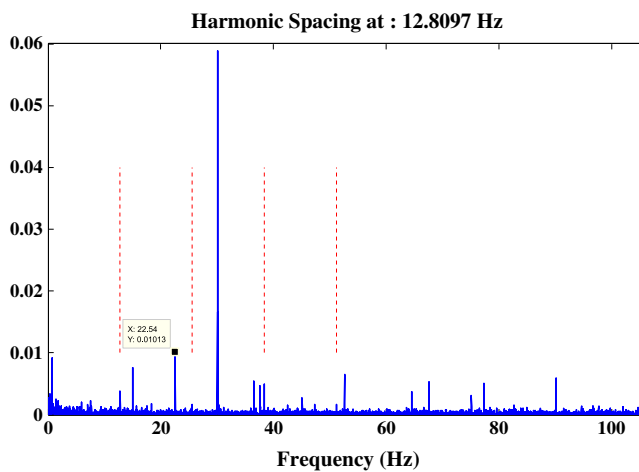


**Figure 8.** Squared envelope spectrum for data 2\_c\_5 sensor AN8 (30 Hz) showing the fundamental train frequency harmonics.

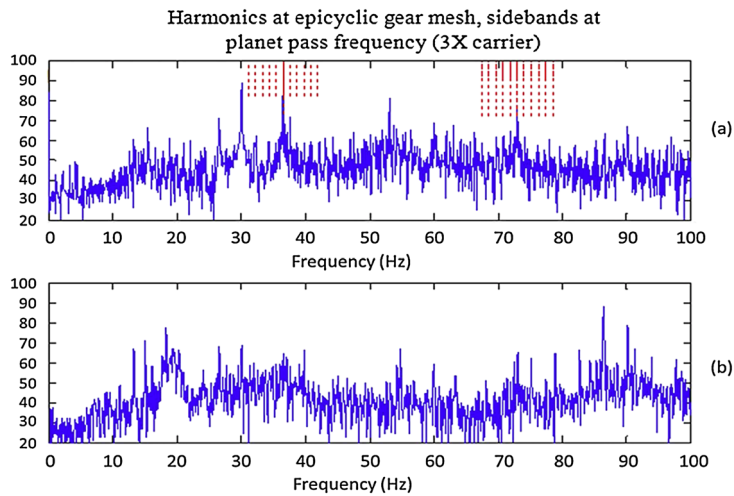
### 3.2.1. Power spectrum and cepstrum comparisons (healthy and faulty signals)

The resolution of the healthy spectra provided was determined and then used to find the equivalent FFT size to use with the faulty data for comparison. Comparisons show increases at the gear mesh frequencies and in sideband families. This was shown clearly for all sensors (AN3, AN5, AN6 and AN7: see sensor locations from Figure 1). Harmonic and sideband cursors show dominant components and modulations.

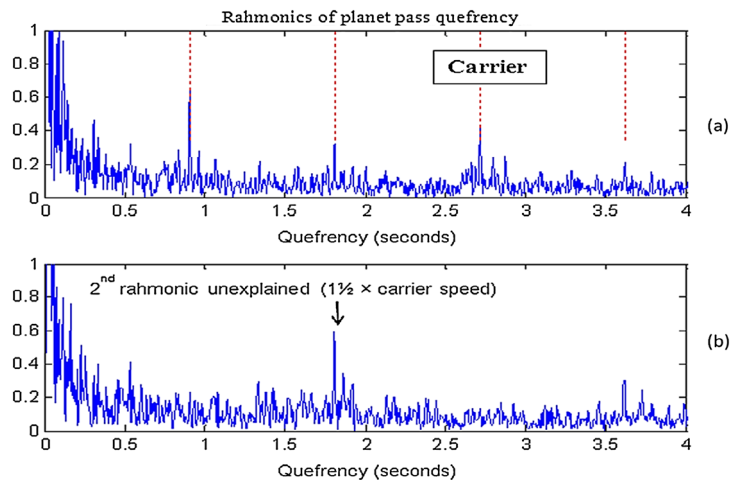
Cepstra were generated from the corresponding spectra to give more information on sideband patterns, thereby simplifying the diagnosis of localized faults. The cepstra represent the amplitude of the analytic cepstrum (the inverse Fourier transform of the one-sided log spectrum<sup>9</sup>). This version can also be used on zoom spectra, as it does not require the spectra to start at zero frequency.

Figure 9 shows the spectrum comparison by using the data from sensor AN3 in the low-speed section of the gearbox. There is a noticeable increase (more than 20 dB) in the HSS component, the epicyclic mesh frequency, and its sidebands. Most noticeable are the sidebands at the planet pass frequency around the epicyclic mesh frequency in the fault case. This is very clear in the cepstrum comparison presented in Figure 10. Note the second rahmonic in the healthy case, corresponding to 1½ times the carrier speed, which is unexplained. It is possible that it has something to do with the 'far from hunting tooth' design of the planetary section and means that the particular tooth combinations occur much more frequently than usual.

In Figures 11 and 12, the spectrum and cepstrum comparisons on the basis of the data from sensor AN5, with generator speed 30 Hz, are presented. The fact that the cepstrum does not change appreciably shows that modulation at ISS (which would come from local faults) did not occur, and the corresponding lack of sidebands in the faulty spectrum confirms that



**Figure 9.** Spectrum comparison by using the data from sensor 3: (a) faulty case and (b) healthy case.



**Figure 10.** Cepstrum comparison by using the data from sensor AN3: (a) faulty case and (b) healthy case.

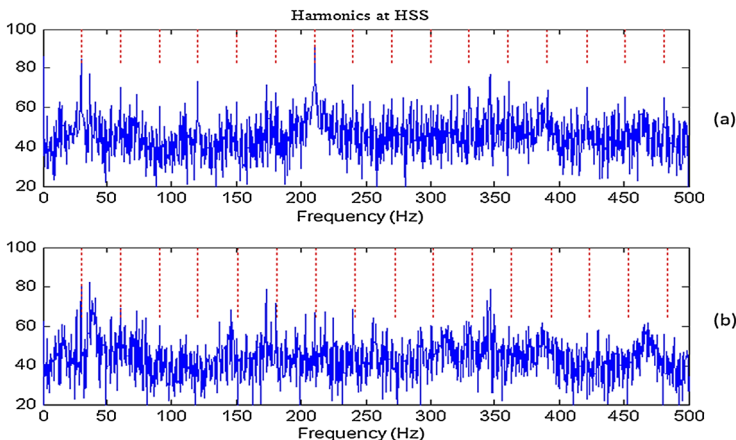


**Figure 11.** Spectrum comparison by using the data from sensor AN5: (a) faulty case and (b) healthy case.

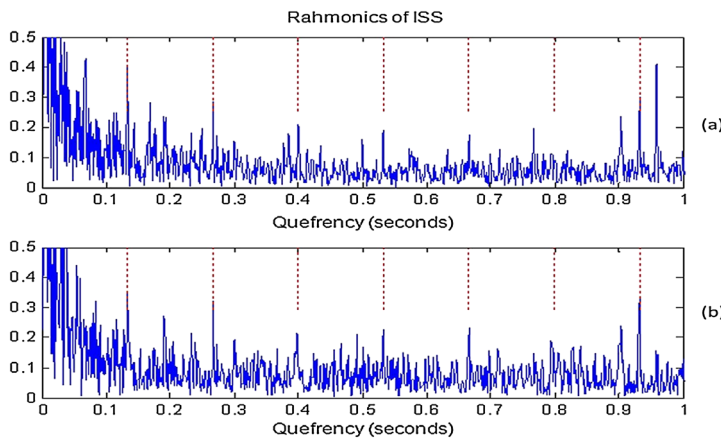


**Figure 12.** Cepstrum comparison by using the data from sensor 5: (a) faulty case and (b) healthy case.

the faults are distributed. Note in particular that the cepstra in Figure 12 are completely different from those in Figure 10, because they are obtained from spectra covering a range of 0–500 Hz rather than 0–100 Hz. The importance of this point in separating the diagnostic information in different frequency ranges has not previously been reported.

Figure 13 dominantly shows the growth of the HSS gear mesh harmonics, and sidebands around them, which are spaced at the HSS. The corresponding cepstra of Figure 14 show that the local faults causing the sideband generation have grown from nothing in the healthy condition, whereas the increased peak corresponding to the ISS probably indicates some growth of other harmonics at this shaft speed because the sidebands around the gear mesh frequencies, in particular the IS gear mesh, were not in evidence. Both the HS pinion and gear had localized scuffing, which would explain the strong modulation at HSS speed.

The distributed wear of the intermediate-shaft pinion, ascribed in the inspection report to the hunting tooth ratio, can also be seen in Figure 13 in the growth of the highlighted harmonics of the ISS gear mesh, without the modulation sidebands that would be present if the faults were more localized. Once again, the cepstra in Figure 14, from spectra covering a range of 0–2000 Hz, show completely different information from those in Figures 10 and 12.

**3.2.1.1. AN6 intermediate-speed shaft signal processed to remove effects of high-speed shaft.** Because the ratio is exactly 4:1, it was difficult to completely separate the effects of the HSS and ISS. However, two procedures were found to be quite successful. In the first, the ISS record was divided into four sections, which were averaged, recombined

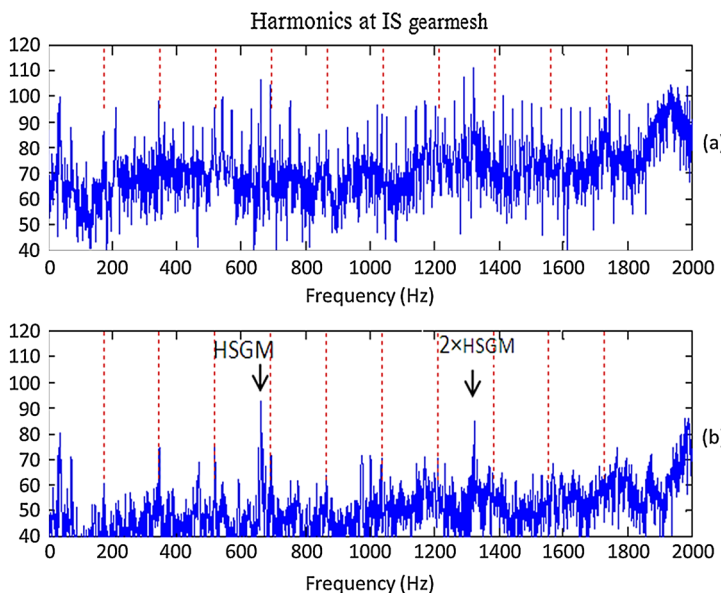


**Figure 13.** Spectrum comparison by using the data from sensor 6: (a) faulty case and (b) healthy case.

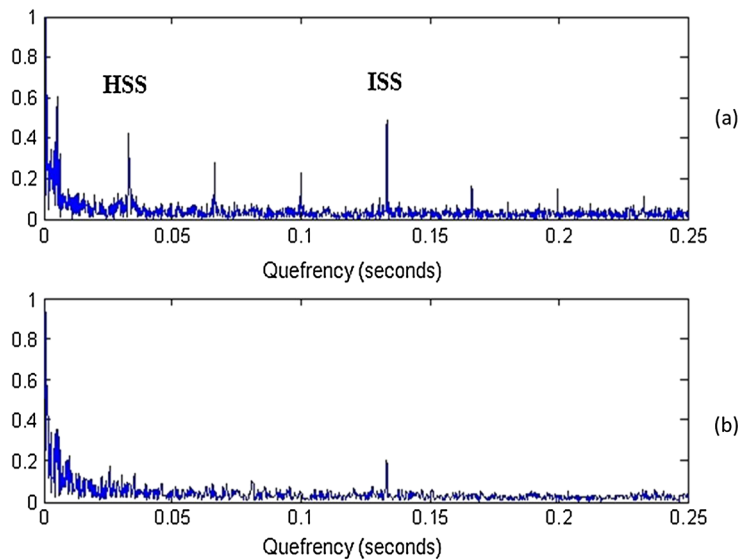


**Figure 14.** Cepstrum comparison by using the data from sensor 6: (a) faulty case and (b) healthy case.

(i.e. repeated four times), and subtracted. The residual record should contain only information from the ISS, for example, the shaft harmonics that are not divisible by four and the ISS gear mesh frequency ( $23\times$ ). Time signals and spectra are shown in Figures 15 and 16.

The HSS gear mesh is strongly modulated by the ISS, because damage is more localized. The ISS gear mesh is very distorted, with many harmonics, but it is not modulated. This is compatible with the distributed damage attributed in the inspection report to the hunting tooth design.

More recently, another approach has been used to separate the two shafts on the basis of liftering (editing) in the cepstrum.<sup>11</sup> Figure 17 shows the results of liftering in the cepstrum of Figure 14(a) to remove rahmonics of the HSS (though including a small amount from the ISS).

Figure 18 compares the spectra before and after this operation, which can be compared with those of Figure 16. It is clear that the cepstral method gives much better resolution than the other one. It should be noted that even though Figure 18 shows only the spectra, the method described in<sup>11</sup> produces the time signals from which those spectra were generated. Another point is that it did not require the original time signals to be synchronously averaged, as did the results of Figure 16.

### 3.2.2. Planetary gear signatures extracted using patented Defence Science and Technology software

Signatures for each planet and the sun gear were extracted by shifted and weighted averages of signals taken as the various planets pass the measurement point.<sup>12</sup> Note that the signature for each planet tooth is actually a composite of the

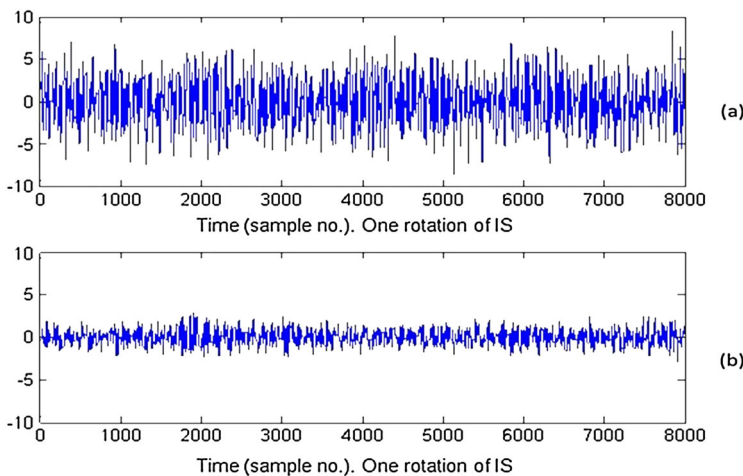


**Figure 15.** Time records from the averaged intermediate-speed shaft (ISS) signals. (a) Original, including four rotations of the high-speed shaft. (b) Residual after removal of the high-speed shaft average.

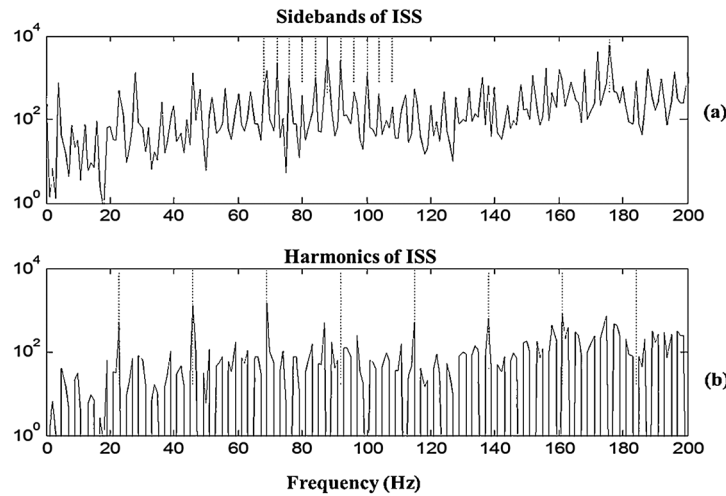


**Figure 16.** Spectra of signals of Figure 13. (a) Original including four rotations of the high-speed shaft. (b) Residual after removal of the high-speed shaft average.

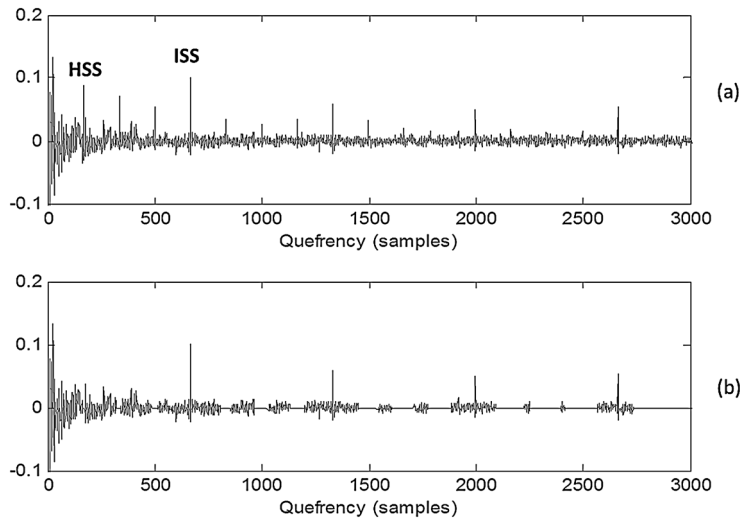


**Figure 17.** Cepstra of the intermediate-speed shaft (ISS) signal before (a) and after (b) the application of a notch lifter to remove high-speed shaft (HSS) harmonics.

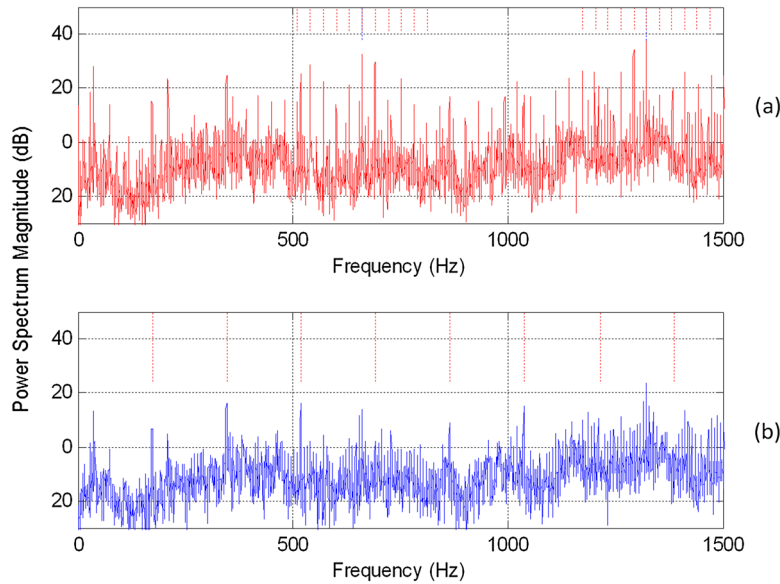
two teeth that mesh simultaneously with the annulus and sun gears (opposite flanks). This is an important observation because no faults were reported on the planet gears, even though virtually all round robin partners detected apparent faults corresponding to the planet gear rotation period. This is discussed further later.

The DSTO patented method described in<sup>12</sup> and illustrated in Figure 19 produces average time signals for each individual planet gear and the sun gear by using shifted weighted signals from passage of each planet past the transducer, with correction for the phase offset of individual teeth for each passage. Note that the average for the sun gear can include the contact of individual teeth with all planet gears.

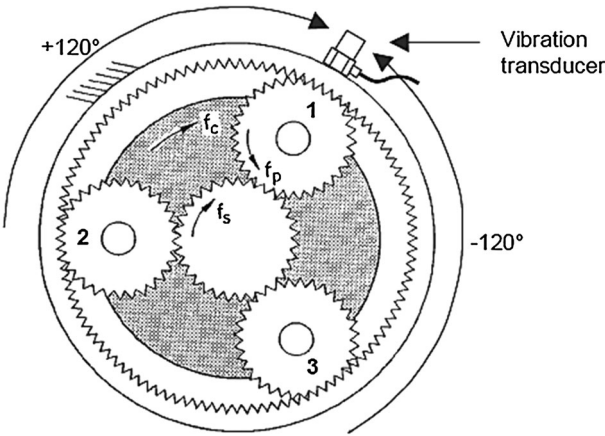
The residual mentioned in some of the following figures is the result of removing the regular tooth mesh signal<sup>8</sup> so as to highlight local faults on a gear.

Figure 20 shows the residual signal for the sun gear at HS and load. This result is compatible with the observation of the inspection report that the sun gear had localized fretting corrosion. Even at a very different speed and load, in Figure 21, the sun gear signature is almost identical (though displaced, because there is no common phase reference). The same was found for the individual planet gear signatures discussed later in Figure 22.

Several round robin partners found evidence of faults on the planet gears, even though none were reported in the inspection report, but the previous figure implies that the fault patterns are the same on all three planets. This could be caused by the 'far from hunting tooth' design of the planetary section. Individual pairs of teeth on the annulus and sun gears, both



**Figure 18.** Log spectra corresponding to the cepstra of Figure 15(a) Original signal. Harmonics at high-speed gear mesh. Sidebands at high-speed shaft. (b) Liftered signal. Harmonics at intermediate-speed pinion mesh frequency.



**Figure 19.** Phase shifts for separated sun gear averages.

of which had faults, could mesh simultaneously on opposite sides of a given planet gear relatively frequently. It would be natural for this to occur identically for all three planets, because all tooth numbers are divisible by three. This potential explanation should be confirmed by more detailed analysis of the kinematics of this particular configuration.

Figure 23 shows a typical average signal for the annulus gear. The residual in this case did not clarify the local faults to any great extent. However, the visible variations are compatible with the results of the inspection report, which found a distributed fault pattern from a local area of scuffing. Because of the numbers of teeth of all planetary components being divisible by three, the damage tended to imprint on every third tooth, and many examples of this pattern over groups of three teeth can be seen in the figure. It seems strange that the inspection report discusses

*scuffing damage on the teeth of the ANN. The root cause of the damage was probably trapping of debris between a pair of teeth. The damage was imprinted on every third tooth of the ANN gear because the gearset had a non-hunting gear ratio with a common factor of three.*

How could this damage have been transferred except via the medium of the planet gears, but no damage was reported on them? Could debris have adhered to a planet tooth without damaging it, or were planet gear teeth distorted without obvious surface damage? This question has not been resolved.

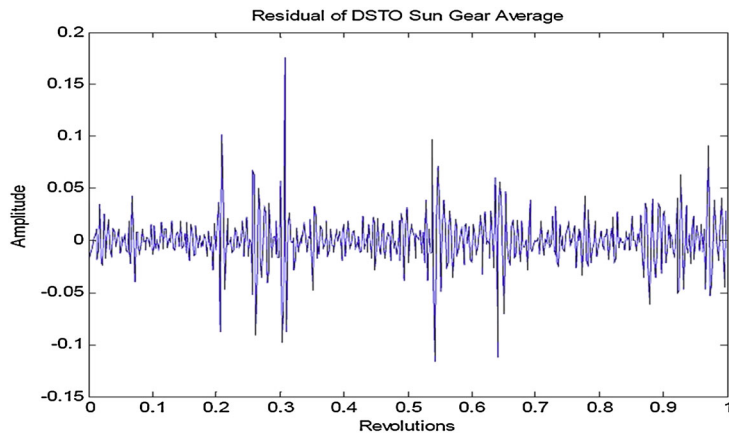


**Figure 20.** Sun gear – residual of Defence Science and Technology average data set 2c (high speed and high load).

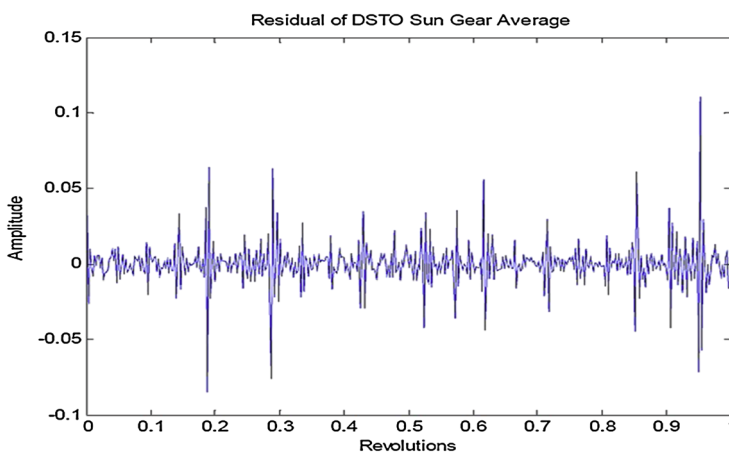


**Figure 21.** Sun gear – residual of Defence Science and Technology average data set 2a (low speed and low load).

#### 4. DISCUSSION, CONCLUSIONS AND LESSONS LEARNED

This paper presents a number of methods, and their combinations, for analysing gear and bearing faults in wind turbine transmissions, characterized by a very wide speed ratio from input to output, and a very low input speed. Most faults that could be expected to change the vibration patterns were picked up. Only one of two faulty bearings (which could have been detected by vibration analysis) was detected. The inner race of the upwind bearing on the intermediate shaft had assembly damage at the roller spacing, debris dents and lines of false brinelling, as well as corrosion at roller spacing, but these were not detected in the vibration analyses. The most likely explanation seems to be that the transmission paths from this bearing to measurement points were not suitable, and other measurement points could perhaps be sought.

Even though there were some indications of faults by inspection of the synchronously averaged time signals in faulty condition, when spectra were received for the gearbox in healthy condition, at about the same time as receiving the inspection report, considerably more detailed analysis could be carried out and more detailed information given for the faults on each gear. An exception was the indication of faults on the planet gears, which were not found on inspection. Most of this later analysis could have been done blind if we had been provided from the outset with the healthy data for comparison.

A more detailed analysis was later performed by Dr David Forrester, of DSTO, using patented algorithms that allow (normally) for the production of separate averages for the individual planet gears and sun gear. These corresponded well with the detected faults on most gears but once again indicated faults on the planet gears. Other round robin partners found the same. It now seems likely that the misdiagnosis was due to the ‘far from hunting tooth’ design of the planetary section, which could mean that faulty teeth on the sun and annulus gears could mesh simultaneously with a healthy planet gear relatively frequently, and thus give an indication of a fault on the planet gear. The fact that the three planets had the same indicated fault pattern lends credence to this interpretation, as the meshing patterns would likely be the same for all three

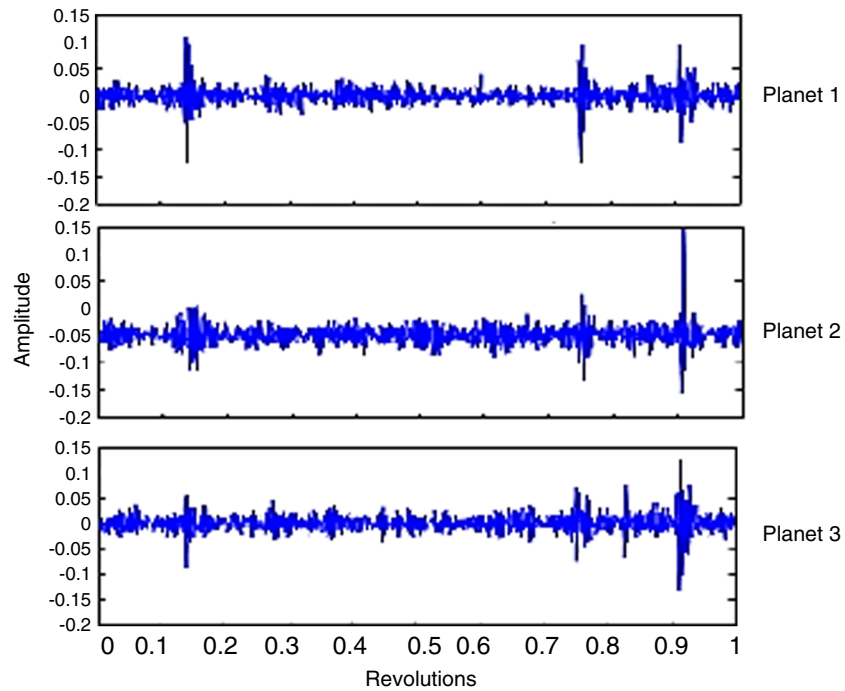


**Figure 22.** Residual signals for the three planet gears.

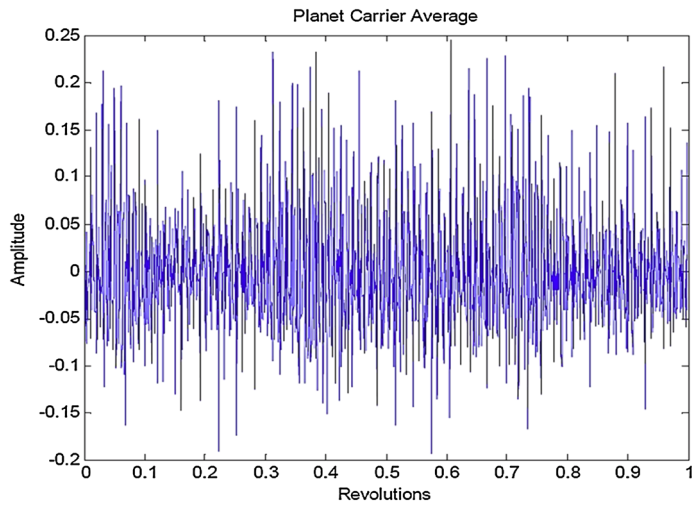


**Figure 23.** Average for the annulus gear.

planets (with all tooth numbers divisible by three). This hypothesis needs to be further investigated before it can be confirmed. This highlighted the fact that gear diagnostics is made easier by the adoption of designs as close as possible to ‘hunting tooth’ designs, which is considered good design practice in any case. The exact 4:1 ratio between the ISS and HSS also made it difficult to separate the faults on gears on these two shafts, although luckily the second mesh on the ISS was a hunting tooth design. Even so, two methods were found that could separate the faults of the gears on the HSS and ISS.

For the relatively modest speed variations in the test data, it was possible to extract information on instantaneous speed from the signals themselves in the form of a pseudo-encoder signal. The signal, typically based on a HS gear mesh component, can be used for order tracking and, thus, synchronous averaging of gear signals throughout the gear train. For larger speed variations, which are not uncommon with pitch controlled wind turbines, it would be necessary to start with a lower order harmonic of the shaft speed; however, the process can be repeated iteratively to improve the speed correction. This should be more fully tested in the future.

## REFERENCES

1. Sawalhi N, Randall RB. Semi-automated bearing diagnostics-three case studies. *Comadem Conference*, Faro, Portugal, Coimbra, Inst. de Telecomunicações, June 13–15 2007.
2. Sawalhi N, Randall RB. Signal Pre-whitening for fault detection enhancement and surveillance in rolling element bearings. *Eight International Conference on Condition Monitoring and Machinery Failure Prevention Technologies*, St David's Hotel, Cardiff, UK, 20–22 June, 2011.
3. Antoni J, Randall RB. Differential diagnosis of gear and bearing faults. *Journal of Vibration and Acoustics* 2002; **124**: 165–171. <http://dx.doi.org/10.1115/1.1456906>
4. Randall RB, Sawalhi N, Coats M. A comparison of methods for separation of deterministic and random signals. *International Journal of Condition Monitoring* 2011; **1**: 11–19. <http://dx.doi.org/10.1784/204764211798089048>
5. Coats MD, Sawalhi N, Randall RB. Extraction of tacho information from a vibration signal for improved synchronous averaging. *Proceedings of Acoustics Australia 2009*, Adelaide, Australia, 23–25 November 2009.
6. Urbanek J, Barszcz T, Sawalhi N, Randall RB. Comparison of amplitude-based and phase-based methods for speed tracking in application to wind turbines. *Metrology and Measurement Systems* 2011; **18**: 295–304.
7. Sawalhi N, Randall RB. Localised fault diagnosis in rolling element bearings in gearboxes. *The Fifth International Conference on Condition Monitoring and Machinery Failure Prevention Technologies*, Edinburgh, UK, July 15–18, 2008, Coxmoor Publishing Company: Oxford, UK, 2008.
8. Wang W, Wong AK. Autoregressive model-based gear fault diagnosis. *Transactions of the ASME, Journal of Vibration and Acoustics* 2002; **124**: 172–179.
9. Randall RB. Vibration-based Condition Monitoring: Industrial, Aerospace and Automotive Applications. Wiley: Chichester, UK, 2011.
10. Ho D, Randall RB. Optimisation of bearing diagnostic techniques using simulated and actual bearing fault signals. *Mechanical Systems and Signal Processing* 2000; **14**: 763–788.
11. Randall RB, Sawalhi N. Cepstral removal of periodic spectral components from time signals. *CMMNO Conference*, Ferrara, Italy, 8–10 May, 2013.
12. Forrester D, Blunt D. Analysis of epicyclic gearbox vibration. *DSTO HUMS Conference*, Melbourne, 2003.
13. Errichello R, Muller J. Gearbox reliability collaborative gearbox 1 failure analysis report. National Renewable Energy Laboratory (NREL), Golden, CO. NREL/SR-5000-530262, 2012. Available: <http://www.nrel.gov/docs/fy12osti/53062.pdf>. (Accessed 18 August 2013)

Copyright of Wind Energy is the property of John Wiley & Sons, Inc. and its content may not be copied or emailed to multiple sites or posted to a listserv without the copyright holder's express written permission. However, users may print, download, or email articles for individual use.